International Science Journal of Engineering & Agriculture
2026; 5(2): 65-80
https://isg-journal.com/isjea
doi: 10.46299/j.isjea.20260502.07
ISSN: 2720-6319

INTERNATIONAL
SCIENCE GROUP

Stress state analysis of semi-infinite layer with cylindrical hinged joint

Igor Arkhypenko
Department of Aircraft Strength, National Aerospace University "Kharkiv Aviation Institute," Kharkiv, Ukraine
ORCID 0009-0009-0311-4437

Serhii Sverdlov
Department of Aircraft Strength, National Aerospace University "Kharkiv Aviation Institute", Kharkiv, Ukraine
ORCID 0009-0001-8220-8731

Olexii Ilin
Department of Aircraft Strength, National Aerospace University "Kharkiv Aviation Institute", Kharkiv, Ukraine
ORCID 0009-0005-7852-9873

Vitaly Miroshnikov
Department of Aircraft Strength, National Aerospace University "Kharkiv Aviation Institute", Kharkiv, Ukraine
ORCID 0000-0002-9491-0181

Petro Fomichev
Department of Aircraft Strength, National Aerospace University "Kharkiv Aviation Institute", Kharkiv, Ukraine
ORCID 0000-0002-5624-4851

Abstract: A spatial problem of elasticity theory has been solved to determine the stress-strain state of a semi-infinite elastic layer containing a cylindrical cavity and an elastic cylindrical pipe (hinged joint). Both cylindrical objects are located parallel to the horizontal boundaries of the layer along the z-axis. The layer is additionally limited by the vertical plane $z=0$, which causes complex spatial edge effects. A distinctive feature of the proposed mathematical model is an original approach to satisfying the conditions at the vertical end of the layer. Instead of directly considering a semi-bounded body, modeling is applied by specifying even or odd (according to the z-coordinate) loads on the horizontal surfaces of an infinite layer. This approach makes it possible to effectively simulate the conditions of a "smooth wall" or "free end." According to the problem statement, normal displacements and tangential stresses are specified on the surface of the cavity and the inner surface of the pipe, and the conditions of smooth contact (equality of normal stresses and displacements in the absence of tangential stresses) are implemented on the surface of the pipe conjugation with the layer. The generalized Fourier method is used to solve the boundary value problem. The displacement vectors for the layer and the pipe are sought as a superposition of the basis solutions of the Lamé equations in Cartesian and local cylindrical coordinate systems. Using addition theorems for the basis solutions, satisfying the boundary conditions is reduced to solving a connected infinite system of linear algebraic equations with respect to unknown spectral and amplitude coefficients. The constructed analytical and numerical apparatus allows us to study with high accuracy the concentration and mutual influence of stresses near the hinge joint and cavity, taking into account the presence of a vertical boundary. The results obtained are important for assessing the strength and reliability of aerospace components and machine-building structures with cylindrical inclusions.

Keywords: semi-infinite layer, cylindrical cavity, elastic pipe, smooth contact, generalized Fourier method, stress-strain state.

1. Introduction

The problem of determining the stress-strain state of structural elements containing cylindrical holes, cavities, or reinforcing elements (pipes, hinges, rivets) is a classic and, at the same time, extremely relevant problem in the mechanics of deformable solids. The reliability of building and machine structures significantly depends on the concentration of stresses arising in the vicinity of such concentrators, especially near the free boundaries of the body.

In real engineering structures, cylindrical inclusions in the form of elastic pipes are most often modeled as plain bearings or guide bushings. These elements are an integral part of hinge joints and are widely used in mechanical engineering, aviation, and construction industries to ensure the mobility of assemblies, reduce wear, and rationally distribute contact loads between the shaft (or axis) and the main body of the part. The durability and safe operation of the entire mechanism directly depends on the strength and reliability of the fit of such elements, especially when they are located near the edges of the structure.

From the point of view of mathematical modeling, the use of an elastic pipe in the layer array allows taking into account the difference in the physical and mechanical properties of the bushing material from the material of the main part. At the same time, the application of ideal smooth contact conditions on the mating surface of the pipe and layer in the boundary problem adequately reflects the physics of a lubricated sliding bearing, where the transmission of normal forces occurs under the condition of minimizing or neglecting tangential stresses (friction forces) at the boundary between the media. Thus, a rigorous analysis of the stress state of such a system makes it possible to identify areas of dangerous stress concentration arising from the interaction of the bushing with the body matrix and the proximity of the free or pinched end.

2. Object and subject of research

The object of the study is elements of machine-building and aerospace structures in the form of a semi-confined thick plate (elastic layer) containing complex cylindrical concentrators in the form of reinforcing elastic bushings (pipes) and free cavities located near the edge of the part (end face).

The subject of the study is the stress-strain state, the patterns of stress distribution, displacements, and their concentration zones in the specified object under the influence of static loading, taking into account the coupling conditions of the system elements.

Geometrically, the object is modeled as an isotropic layer (Fig. 1) with elastic constants E_0 , ν_0 , bounded by horizontal planes $y=h$, $y=-\tilde{h}$ and a vertical end face $z=0$. Inside, along the z-axis parallel to the boundaries, there are:

1. An elastic pipe (E_1, ν_1) with outer R_1 and inner r_1 radii, which simulates a guide bushing or sliding bearing.
2. A cylindrical cavity with radius R_2 (cut cylindrical support).

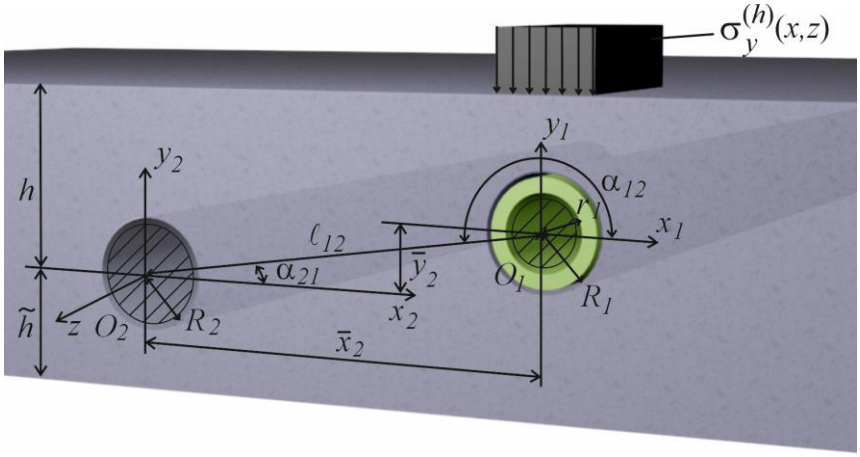

Fig. 1. Layer with a cylindrical cavity and a pipe.

Stresses are specified on the upper and lower boundaries of the layer

$$F\vec{U}(x,z)_{|y=h} = \vec{F}_h^0(x,z),\ F\vec{U}(x,z)_{|y=-\tilde{h}} = \vec{F}_{\tilde{h}}^0(x,z),$$

where

$$\begin{aligned} \vec{F}_h^0(x,z) &= \tau_{yx}^{(h)}\vec{e}_x + \sigma_y^{(h)}\vec{e}_y + \tau_{yz}^{(h)}\vec{e}_z, \\ \vec{F}_{\tilde{h}}^0(x,z) &= \tau_{yx}^{(\tilde{h})}\vec{e}_x + \sigma_y^{(\tilde{h})}\vec{e}_y + \tau_{yz}^{(\tilde{h})}\vec{e}_z. \end{aligned} \tag{1}$$

Smooth contact conditions are specified on the inner surface of the pipe (p = 1)

$$\left.\begin{aligned} U_\rho(\varphi_1,z)_{|\rho_1=r_1} &= U_0^{(1)}(\varphi_1,z) \\ \tau_{\rho\varphi}(\varphi_1,z)_{|\rho_1=r_1} &= \tau_1^{(1)}(\varphi_1,z) \\ \tau_{\rho z}(\varphi_1,z)_{|\rho_1=r_1} &= \tau_2^{(1)}(\varphi_1,z) \end{aligned}\right\}. \tag{2}$$

On the surface of the cylindrical cavity (p = 2), the conditions of smooth contact

$$\left.\begin{aligned} U_\rho(\varphi_2,z)_{|\rho_2=R_2} &= U_0^{(2)}(\varphi_2,z) \\ \tau_{\rho\varphi}(\varphi_2,z)_{|\rho_2=R_2} &= \tau_1^{(2)}(\varphi_2,z) \\ \tau_{\rho z}(\varphi_2,z)_{|\rho_2=R_2} &= \tau_2^{(2)}(\varphi_2,z) \end{aligned}\right\}. \tag{3}$$

At the contact surface between the pipe and the layer (R_1), ideal smooth contact conditions are specified (normal forces and displacements are transmitted continuously, and there are no tangential stresses):

$$\begin{gathered} U_\rho^{(0)}\Big|_{\rho=R} = U_\rho^{(1)}\Big|_{\rho=R} \\ \sigma_\rho^{(0)}\Big|_{\rho=R} = \sigma_\rho^{(1)}\Big|_{\rho=R} \\ \tau_{\rho\phi}^{(0)}\Big|_{\rho=R} = \tau_{\rho\phi}^{(1)}\Big|_{\rho=R} = \tau_{\rho z}^{(0)}\Big|_{\rho=R} = \tau_{\rho z}^{(1)}\Big|_{\rho=R} = 0 \end{gathered}, \quad (4)$$

where $U_\rho^{(0)}$ is the solution for the layer; $U_\rho^{(1)}$ is the solution for the pipe;

$F\vec{U} = 2 \cdot G \cdot \left[\frac{\sigma}{1-2\cdot\sigma} \vec{n} \cdot \mathrm{div}\vec{U} + \frac{\partial}{\partial n}\vec{U} + \frac{1}{2}\left(\vec{n} \times \mathrm{rot}\vec{U}\right) \right]$ is the stress operator.

The end face z=0 simulates the "Free end face" or "Smooth wall" modes. All specified functions decrease rapidly from the origin.

Foreign analogues are typical components of global engineering practice: lug/clevis joints, wing-to-fuselage mounting hinges, lifting equipment boom assemblies. They often use bushings made of special anti-friction alloys (e.g., Oilite) or composites (PTFE) to ensure free sliding in the socket.

Despite their widespread use, the disadvantages of these components in operating conditions are:

1. Edge effect. The proximity of the end face (z=0) causes a sharp concentration of stresses, which provokes the formation of edge cracks.
2. Concentrator interference. The superposition of stress fields from the cavity and the bushing critically weakens the bridge between them.
3. Wear and backlash. Micro-sliding at the boundary of smooth contact under cyclic loads leads to surface wear, backlash, and dangerous dynamic shocks.

3. Purpose and objectives of the study

Based on the identified operational deficiencies of the object, there is a need to accurately determine its stress state.

The purpose of the study is to develop a reliable mathematical model and analytical and numerical methods for calculating the stress-strain state of a semi-confined elastic layer with a cylindrical cavity and a supporting pipe (hinge) to determine the rational parameters of the structure that will minimize stress concentration and ensure its further reliable operation.

To achieve the set goal and update the object, the following research tasks must be solved:

1. Formulate the boundary value problem of elasticity theory for the system "semi-infinite shell – elastic pipe – cavity," adequately describing the conditions of smooth contact at the interface between the sleeve and the shell matrix.

2. Adapt the mirror reflection method by specifying even or odd stresses at the horizontal boundaries of the infinite shell to accurately model the conditions at the vertical end z=0 ("smooth wall" or "free end"). This will allow the boundary effect to be taken into account without directly introducing a complex vertical boundary.

3. Construct an analytical solution of the Lamé equations using the generalized Fourier method, presenting the total displacement field as a superposition of basis solutions in Cartesian and local cylindrical coordinate systems.

4. Reduce the boundary value problem to an infinite system of linear algebraic equations using addition theorems and perform its numerical solution by the reduction method.

5. Perform a numerical analysis of the stress state of the system. Investigate the patterns of distribution of normal and spatial tangential stresses at the boundaries of the matrix and the surfaces of the reinforcing pipe, revealing the influence of the spatial edge effect under symmetric and antisymmetric loads.

6. Localize critical areas of the structure (in particular, the area of the neck between the pipe and the surface of the layer) and, based on the data obtained, justify the practical value of the developed model for improving engineering units, reducing their metal intensity, design costs, and avoiding premature failure.

4. Literature review

The fundamental principles of studying stress distribution near openings and in three-dimensional elastic bodies are laid down in classical works [1–4]. Although approximate numerical approaches, in particular the finite element method (FEM) and corresponding software packages such as Ansys [5, 6], are widely used today to solve engineering problems, the development of rigorous analytical and analytical-numerical methods remains necessary. Analytical solutions allow for in-depth parametric analysis, a better understanding of the physics of wave and static processes, and serve as a benchmark for verifying numerical algorithms.

Significant progress in solving spatial problems for bodies with cylindrical boundaries is associated with the development of the generalized Fourier method [7], which allows the solution of a boundary value problem to be presented as a superposition of basis solutions of the Lamé equation in different coordinate systems. This approach has been successfully applied to the analysis of dynamic and wave processes in an elastic layer with a cavity [8, 9], as well as to the study of stresses in functionally graded plates [10].

A large number of modern studies are devoted to static problems for an infinite elastic layer with cylindrical concentrators. In particular, the first fundamental problem of elasticity theory for a layer with a cavity, the influence of periodic loading, and the presence of several cylindrical supports were considered in [11–14]. Further complication of the models led to the study of the interaction of the layer matrix with elastic inclusions. Problems concerning hinged joints and the presence of reinforcing pipes with different contact conditions (smooth contact, rigid coupling) are presented in publications [15–19].

The vast majority of the above-mentioned works consider the model of an infinite layer. Taking into account an additional vertical boundary (end face), which transforms the layer into a semi-bounded one, significantly complicates the mathematical formulation due to the emergence of spatial edge effects in the corner zones of the body. An effective mathematical technique for overcoming this complexity is the mirror reflection method. The essence of the method is to reduce the problem for a semi-bounded body to an equivalent problem for an infinite body by symmetrical (or antisymmetrical) extension of the geometry and boundary conditions relative to the cut plane z=0. Recently, this conceptual approach has been successfully applied in works [20, 21] to solve the spatial problem of elasticity theory for a semi-bounded layer with a given symmetric load.

The purpose of this work is to further develop the generalized Fourier method and the mirror reflection method for analyzing the stress state of a semi-bounded layer that simultaneously contains a free cylindrical cavity and an elastic cylindrical pipe. A realistic model of a hinged joint with smooth contact conditions between the pipe and the layer is considered, which allows investigating the mutual influence of concentrators and edge effects from a free or smoothly clamped vertical end.

5. Problem statement

To achieve the set goal and improve the object (minimizing stress concentration in the hinge joint near the edge), strict analytical and numerical-analytical methods of spatial elasticity theory are used in the work.

The main equation describing the stress-strain state of an isotropic elastic body in the absence of mass forces is the vector Lamé equation in displacements:

$$(1-2\nu)\Delta\vec{U} + \operatorname{grad}\operatorname{div}\vec{U} = 0$$

where U is the displacement vector, ν is the Poisson's ratio of the material, and Δ is the Laplace operator. This equation is applied both to the matrix material of the layer and to the elastic pipe with the corresponding elastic constants.

To solve the corresponding boundary value problem, the following set of methods and approaches is used:

1. Generalized Fourier method [7]. Basic analytical research method. It consists in representing the desired displacement vector for the layer matrix and pipe as the sum of partial (basis) solutions of the Lamé equation. For the layer, a superposition of plane harmonics in the Cartesian coordinate system and cylindrical vector harmonics (singular solutions that decay at infinity) is used. The basis solutions of the Lamé equation $\vec{u}_k^{(+)}$, $\vec{u}_k^{(-)}$, $\vec{S}_{k,m}$, $\vec{R}_{k,m}$ are presented in the form [7]:

$$\vec{u}_k^{\pm}(x,y,z;\lambda,\mu) = N_k^{(d)} e^{i(\lambda z+\mu x)\pm\gamma y};$$

$$\vec{R}_{k,m}(\rho,\varphi,z;\lambda) = N_k^{(p)} I_m(\lambda\rho) e^{i(\lambda z+m\varphi)};$$

$$\vec{S}_{k,m}(\rho,\varphi,z;\lambda) = N_k^{(p)}\left[(\operatorname{sign}\lambda)^m K_m(|\lambda|\rho)\cdot e^{i(\lambda z+m\varphi)}\right]; k=1,2,3;$$

$$N_1^{(d)} = \frac{1}{\lambda}\nabla;\ N_2^{(d)} = \frac{4}{\lambda}(\nu-1)\vec{e}_2^{(1)} + \frac{1}{\lambda}\nabla(y\,\cdot)\ ;\ N_3^{(d)} = \frac{i}{\lambda}\operatorname{rot}\left(\vec{e}_3^{(1)}\,\cdot\right);$$

$$N_1^{(p)} = \frac{1}{\lambda}\nabla\ ;\ N_2^{(p)} = \frac{1}{\lambda}\left[\nabla\left(\rho\frac{\partial}{\partial\rho}\right) + 4(\nu-1)\left(\nabla - \vec{e}_3^{(2)}\frac{\partial}{\partial z}\right)\right];$$

$$N_3^{(p)} = \frac{i}{\lambda}\operatorname{rot}\left(\vec{e}_3^{(2)}\,\cdot\right);$$

$$\gamma = \sqrt{\lambda^2+\mu^2},\ -\infty < \lambda,\mu < \infty,$$

where ν is Poisson's ratio; $I_m(x)$, $K_m(x)$ are modified Bessel functions.

A combination of regular and singular cylindrical solutions is used for the pipe.

2. Mirror reflection method [20]. A specific technique for modeling the vertical end face z=0. Instead of solving the problem for a semi-bounded body, an infinite layer is considered. On its horizontal surfaces $y=h$ and $y=-\tilde{h}$, stresses are specified as even or odd functions of the z coordinate. Due to the symmetry (or antisymmetry) of the problem, the conditions of a "smooth wall" (absence of normal displacements and tangential stresses) or a "free end face" (absence of normal and tangential stresses) are automatically satisfied on the plane z=0.

3. Addition theorem apparatus [7]. Used to transition between different coordinate systems. Since the boundary conditions are specified on surfaces described in different systems (planes y=const and cylinders ρ=const), McDonald's integral representations and the relationship between cylindrical functions allow the basis solutions to be rearranged from one coordinate system to another.

The formulas for transition between the basis solutions of the Lamé equation are applied in the form [7].

Transition from external solutions for the cylinder $\vec{S}_{k,m}$ to solutions for the layer $\vec{u}_k^{(-)}$ (when y > 0) and $\vec{u}_k^{(+)}$ (when y < 0):

$$\vec{S}_{k,m}(\rho,\varphi,z;\lambda)=\frac{(-i)^m}{2}\int_{-\infty}^{\infty}\omega_{\mp}^{m}\cdot\vec{u}_k^{(\mp)}\cdot\frac{d\mu}{\gamma},\ \ k=1,\ 3;$$

$$\vec{S}_{2,m}(\rho,\varphi,z;\lambda)=\frac{(-i)^m}{2}\int_{-\infty}^{\infty}\omega_{\mp}^{m}\cdot\left(\left(\pm m\cdot\mu-\frac{\lambda^2}{\gamma}\right)\vec{u}_1^{(\mp)}-\lambda^2\vec{u}_2^{(\mp)}+\right. \tag{5}$$

$$\left.\pm4\mu(1-\nu)\vec{u}_3^{(\mp)}\right)\frac{d\mu}{\gamma^2},$$

where $\gamma=\sqrt{\lambda^2+\mu^2}$, $\omega_{\mp}(\lambda,\mu)=\frac{\mu\mp\gamma}{\lambda}$, $m=0,\pm1,\pm2,\ldots$;

Transition from solutions of the layer to internal solutions of the cylinder $\vec{R}_{k,m}$:

$$\vec{u}_k^{(\pm)}(x,y,z)=\sum_{m=-\infty}^{\infty}\left(i\cdot\omega_{\mp}\right)^m\vec{R}_{k,m},\ \ (k=1,\ 3);$$

$$\vec{u}_2^{(\pm)}(x,y,z)=\sum_{m=-\infty}^{\infty}\left[\left(i\cdot\omega_{\mp}\right)^m\cdot\lambda^{-2}\left((m\cdot\mu)\cdot\vec{R}_{1,m}\pm\right.\right. \tag{6}$$

$$\left.\left.\pm\gamma\cdot\vec{R}_{2,m}+4\mu(1-\nu)\vec{R}_{3,m}\right)\right]\ ,$$

where

$$\vec{R}_{k,m}=\vec{\tilde{b}}_{k,m}(\rho,\lambda)\cdot e^{i(m\varphi+\lambda z)};$$

$$\vec{\tilde{b}}_{1,n}(\rho,\lambda)=\vec{e}_\rho\cdot I_n'(\lambda\rho)+i\cdot I_n(\lambda\rho)\cdot\left(\vec{e}_\varphi\frac{n}{\lambda\rho}+\vec{e}_z\right);$$

$$\vec{\tilde{b}}_{2,n}(\rho,\lambda)=\vec{e}_\rho\cdot\left[(4\nu-3)\cdot I_n'(\lambda\rho)+\lambda\rho_p I_n''(\lambda\rho)\right]+$$

$$+\vec{e}_\varphi i\cdot m\left(I_n'(\lambda\rho)+\frac{4(\nu-1)}{\lambda\rho}I_n(\lambda\rho)\right)+\vec{e}_z i\lambda\rho I_n'(\lambda\rho);$$

$$\vec{\tilde{b}}_{3,n}(\rho,\lambda)=-\left[\vec{e}_\rho\cdot I_n(\lambda\rho)\frac{n}{\lambda\rho}+\vec{e}_\varphi\cdot i\cdot I_n'(\lambda\rho)\right];$$

$\vec{e}_\rho$, $\vec{e}_\varphi$, $\vec{e}_z$ – orths in the cylindrical coordinate system;

Transition from solutions of cylinder number *p* to solutions of cylinder number *q*:

$$\vec{S}_{k,m}(\rho_p,\varphi_p,z;\lambda)=\sum_{n=-\infty}^{\infty}\vec{b}_{k,pq}^{mn}(\rho_q)\cdot e^{i(n\varphi_q+\lambda z)},k=1,\ 2,\ 3; \tag{7}$$

$$\vec{b}_{1,pq}^{mn}(\rho_q)=(-1)^n\tilde{K}_{m-n}(\lambda\ell_{pq})\cdot e^{i(m-n)\alpha_{pq}}\cdot\vec{\tilde{b}}_{1,n}(\rho_q,\lambda);$$

$$\vec{b}^{mn}_{3,pq}\left(\rho_q\right)=(-1)^n\,\tilde{K}_{m-n}\left(\lambda\ell_{pq}\right)\cdot e^{i(m-n)\alpha_{pq}}\cdot\vec{\tilde{b}}_{3,n}\left(\rho_q,\lambda\right);$$

$$\vec{b}^{mn}_{2,pq}\left(\rho_q\right)=(-1)^n\left\{\tilde{K}_{m-n}\left(\lambda\ell_{pq}\right)\cdot\vec{\tilde{b}}_{2,n}\left(\rho_q,\lambda\right)-\frac{\lambda}{2}\ell_{pq}\cdot\right.$$

$$\left.\cdot\left[\tilde{K}_{m-n+1}\left(\lambda\ell_{pq}\right)+\tilde{K}_{m-n-1}\left(\lambda\ell_{pq}\right)\right]\cdot\vec{\tilde{b}}_{1,n}\left(\rho_q,\lambda\right)\right\}\cdot e^{i(m-n)\alpha_{pq}},$$

α_{pq} – angle between axis x_p and segment ℓ_{qp} ; $\tilde{K}_m\left(x\right)=\left(sign\left(x\right)\right)^m\cdot K_m\left(\left|x\right|\right)$.

4. Reduction method. Used for numerical solution of the obtained infinite system of linear algebraic equations. The system is truncated to a finite size, which ensures the necessary accuracy of calculations of the sought decomposition coefficients.

6. Research results

6.1. Creation and solution of a system of equations

The Lamé equation is presented in the form proposed in [16]:

$$\vec{U}^{(0)}=\sum_{p=1}^{2}\sum_{k=1}^{3}\int_{-\infty}^{\infty}\sum_{m=-\infty}^{\infty}B^{(p)}_{k,m}(\lambda)\cdot\vec{S}_{k,m}\left(\rho_p,\varphi_p,z;\lambda\right)d\lambda+$$

$$+\sum_{k=1}^{3}\int_{-\infty}^{\infty}\int_{-\infty}^{\infty}\left(H_k\left(\lambda,\mu\right)\cdot\vec{u}_k^{(+)}\left(x,y,z;\lambda,\mu\right)+\tilde{H}_k\left(\lambda,\mu\right)\cdot\vec{u}_k^{(-)}\left(x,y,z;\lambda,\mu\right)\right)d\mu d\lambda, \quad (8)$$

$$\vec{U}^{(1)}=\sum_{k=1}^{3}\int_{-\infty}^{\infty}\sum_{m=-\infty}^{\infty}A^{(1)}_{k,m}(\lambda)\cdot\vec{R}_{k,m}\left(\rho_1,\varphi_1,z;\lambda\right)+\tilde{A}^{(1)}_{k,m}(\lambda)\cdot\vec{S}_{k,m}\left(\rho_1,\varphi_1,z;\lambda\right)d\lambda, \quad (9)$$

where $H_k\left(\lambda,\mu\right)$, $\tilde{H}_k\left(\lambda,\mu\right)$, $B^{(1)}_{k,m}(\lambda)$, $B^{(2)}_{k,m}(\lambda)$, $A^{(1)}_{k,m}(\lambda)$, $\tilde{A}^{(1)}_{k,m}(\lambda)$ are 18 unknown functions (k = 1..3) that must be found from boundary conditions (1) – (3) and conjugation conditions (4).

The procedure for determining the eighteen unknown spectral and amplitude functions in decompositions (8) and (9) boils down to constructing and solving a system of 18 integro-algebraic equations. This system is formed by sequentially satisfying the boundary conditions on all surfaces of the body under study:

The first block of six equations is formed from the satisfaction of boundary conditions on the horizontal flat surfaces of layer (1). For this purpose, the general solution (8) is acted upon by the corresponding matrix stress operator, and the given external loads (1) are decomposed into a double Fourier integral. For correct comparison, the basic solutions from the cylindrical coordinate system are transformed into Cartesian coordinates using addition theorems and transition formulas (5), after which the obtained expressions are equated.

The second block of three equations follows from the boundary conditions on the contour of a free cylindrical cavity (3). The given conditions are decomposed into a Fourier integral along the z-axis and a Fourier series in the polar angle φ. The stress operator is applied to the displacement vector (8) to form the corresponding relationships in displacements and stresses. In this case, the basis

solutions from the Cartesian coordinate system are converted to the local cylindrical coordinate system using the transition formulas (6).

The following three equations are obtained by satisfying the conditions at the inner boundary of the elastic pipe (2). The pipe displacement vector (9) is differentiated by the stress operator for to find the corresponding components, which are then equated to the given functions (2), previously presented in the form of a Fourier integral along the z-axis and a Fourier series along the angle φ.

The last six equations are generated from the conditions of smooth contact at the boundary between the layer matrix and the outer surface of the pipe (4). To satisfy these conditions, the Cartesian basis solutions are rewritten in the local cylindrical coordinate system of the pipe using formulas (5). In addition, transition theorems (7) are used to translate the basis solutions from one local cylindrical coordinate system (cavity) to another (pipe).

At the algebraization stage, the unknown coefficients of plane harmonics are expressed in terms of the spectral densities of cylindrical functions from the first six equations (conditions at plane boundaries) and substituted into the remaining equations. By equating the coefficients for the same basis functions and eliminating the integrals and trigonometric series in the left and right parts, the original integro-algebraic system is reduced to an infinite system of linear algebraic equations of the second kind.

The resulting system of 12 equations is completely regular, which allows the reduction method (truncation to finite order) to be effectively applied to it. As a result of the numerical solution, the unknown amplitude coefficients for cylindrical harmonics are found. The found values are substituted into the previously derived expressions for plane harmonics, which allows us to retrospectively calculate all unknown parameters of the problem and completely determine the stress-strain state of the system.

6.2. Numerical studies of the stress state

Numerical results obtained for a layer of D16T alloy, Poisson's ratio ν_0= 0.3, modulus of elasticity E_0= $7.1\cdot10^4$ MPa. Physical characteristics of the pipe: steel, Poisson's ratio ν_1 = 0.25, modulus of elasticity $E_1 = 2\cdot10^5$ MPa.

Geometric parameters of the model: the cylindrical cavity and the pipe are located on the same horizontal axis (α_{12}=0), the distance between the cavity and the pipe is ℓ_{12}= 100 mm, the radius of the cavity and the outer radius of the pipe $R_1 = R_2 = 15$ mm, the inner radius of the pipe $r_2 = 8$ mm, the distances to the upper and lower boundaries of the layer $h = \tilde{h} = 25$ mm.

On the inner surface of the pipe ($p = 1$), the conditions of smooth contact are specified

$$U_0^{(1)}(\varphi_1, z) = \tau_1^{(1)}(\varphi_1, z) = \tau_2^{(1)}(\varphi_1, z) = 0.$$

Smooth contact conditions are specified on the surface of the cylindrical cavity

$$U_0^{(2)}(\varphi_2, z) = \tau_1^{(2)}(\varphi_2, z) = \tau_2^{(2)}(\varphi_2, z) = 0.$$

At the upper boundary of the layer, the stresses are specified in the symmetry variant:

$$\sigma_y^{(h)}(x, z) = \begin{cases} -10^4 \cdot \left(x^2 + 10^2\right)^{-2}, -20 \le z \le 20 \\ 0, |z| > 20 \end{cases}$$

and in the antisymmetry variant

$$\sigma_y^{(h)}(x,z)=\begin{cases}-10^4\cdot\left(x^2+10^2\right)^{-2}, 0<z\le 20\\ 10^4\cdot\left(x^2+10^2\right)^{-2}, -20\le z<0.\\ 0, |z|>20\end{cases}$$

At the lower boundary of the layer, the stresses are given as $\tau_{yx}^{(\tilde{h})}=\sigma_y^{(\tilde{h})}=\tau_{yz}^{(\tilde{h})}=0$.

Fig. 2 shows the distribution of normal stresses σ_x and σ_z at the upper flat boundary of the layer depending on the distance along the z-axis at x=0, given symmetry and antisymmetry.

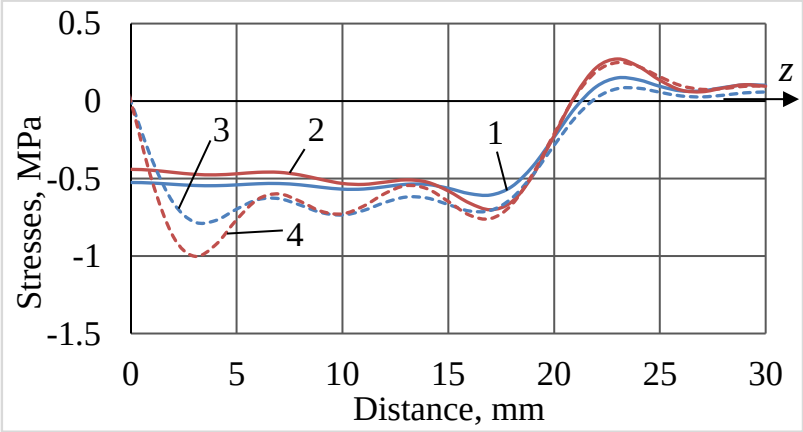

Fig. 2. Stress state at the upper boundary of the layer: 1 – σ_x, symmetry; 2 – σ_z, symmetry; 3 – σ_x, antisymmetry; 4 – σ_z, antisymmetry.

Analysis of the curves for two load options (Fig. 2) reveals significant differences in the stress state, especially near the vertical edge (in the 0–10 mm zone).

In the case of symmetrical loading, which simulates the conditions of a "smooth wall" (Fig. 2, solid curves 1 and 2), the stresses σ_x and σ_z at the end start from non-zero values and are distributed relatively evenly, without sharp jumps in the edge zone.

However, with an antisymmetric load simulating a "free end" (Fig. 2, dashed curves 3 and 4), a pronounced edge effect is observed. Normal stresses increase sharply in magnitude, reaching local compression maxima at a short distance from the edge (about 3–4 mm). In particular, the stress σ_z (curve 4) at this point reaches -1.0 MPa, which is more than twice the corresponding values for the symmetric case in the same zone. This confirms that the presence of a load-free vertical boundary leads to a significant local concentration of stresses.

Fig. 3 illustrates the angular distribution of the normal components of the stress tensor (σ_ρ, σ_φ, σ_z) on the inner free surface of the reinforcing pipe depending on the polar angle.

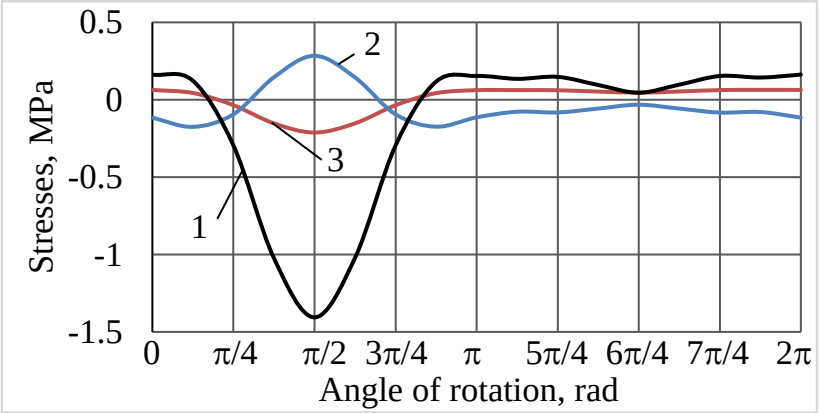

Fig. 3. Stress state on the inner surface of the pipe: 1 – σ_ρ ; 2 – σ_φ ; 3 – σ_z.

Radial stresses σ_r (Fig. 3, curve 1) show the most pronounced dynamics. In the vicinity of the angle $\pi/2$ (which usually corresponds to the direction of the external load or the zone of maximum compression), there is a sharp peak in compressive stresses, which reach a value of -1.407 MPa. In the remaining areas (from π to 2π), radial stresses stabilize and acquire insignificant positive values (0.163 MPa), which may indicate insignificant local detachment or peculiarities of contour deformation.

The hoop stresses σ_φ (Fig. 3, curve 2) are opposite in nature to the radial stresses in the most loaded zone. At the point of maximum radial compression (at an angle of $\pi/2$), the hoop stresses reach their maximum tensile value of +0.285 MPa. This is a classic manifestation of the Poisson effect and bending of a curved wall: intense compression of the pipe along one axis causes its internal fibers to stretch in a perpendicular direction.

Longitudinal stresses σ_z (Fig. 3, curve 3) are the least intense compared to other components. They fluctuate within a very narrow range, reaching a local minimum (-0.211 MPa) also in the vicinity of the angle $\pi/2$. Their insignificant amplitude is explained by the fact that the inner surface of the pipe is free from axial fastenings, and the main deformation occurs in the cross-section plane.

In general, the graph confirms that the inner surface of the pipe undergoes intense local bending and compression, with the area near the angle $\pi/2$ being the most dangerous in terms of strength.

Fig. 4 shows the angular distribution of the normal components of the stress tensor (σ_r, σ_φ, σ_z) on the outer surface of the reinforcing pipe (R_1 =15 mm). This surface is the boundary of ideal smooth contact between the steel sleeve (E_1) and the aluminum layer (E_0).

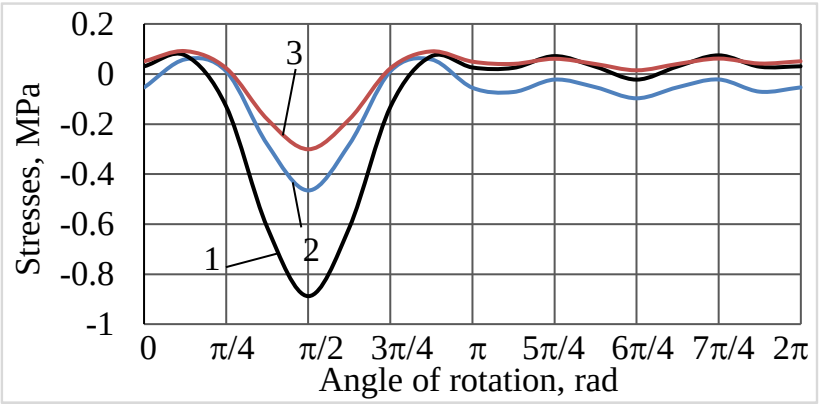

Fig. 4. Stress state on the outer surface of the pipe: 1 – σ_ρ ; 2 – σ_φ ; 3 – σ_z.

A comparative analysis of the stress state of the upper (Fig. 3) and lower (Fig. 4) boundaries reveals a significant change in the nature of the stress state across the pipe wall thickness:

Radial stresses σ_r (Fig. 4, curve 1), in accordance with the conditions of smooth contact, are transmitted continuously from the layer to the pipe. The graph shows that the zone of maximum

compression is also localized in the vicinity of the angle π/2, where the stresses reach a value of -0.8875 MPa. It should be noted that in terms of modulus, they are smaller than on the inner surface (where it was -1.407 MPa), which indicates a gradual decay of contact pressure as it penetrates deeper into the pipe mass.

The hoop stresses σ_φ (Fig. 4, curve 2) demonstrate radically different behavior compared to the inner surface. If tensile stress was observed on the inner contour at π/2, then compressive stresses reaching -0.46529 MPa occur on the outer surface at the same point. Such a change in the sign of σ_φ across the cross-section thickness is a classic sign of thick-walled shell bending: the inner fibers are stretched, and the outer fibers are compressed under the action of external pressure from the matrix.

Longitudinal stresses σ_z (Fig. 4, curve 3) have a qualitatively similar distribution to hoop and radial stresses. The maximum compression (about -0.3 MPa) is also recorded at an angle of π/2.

A distinctive feature of the stress state at this boundary is that in the zone of maximum load (π/2), a state of triaxial compression is realized (all three components are negative). confirms that the rigid steel sleeve (since $E_1 > E_0$) accumulates a significant part of the mechanical energy, unloading the adjacent areas of the less rigid aluminum layer.

The angular distribution of spatial tangential stresses $\tau_{\varphi z}$ on the inner and outer surfaces of the reinforcing steel pipe under antisymmetry conditions is shown in Fig. 5.

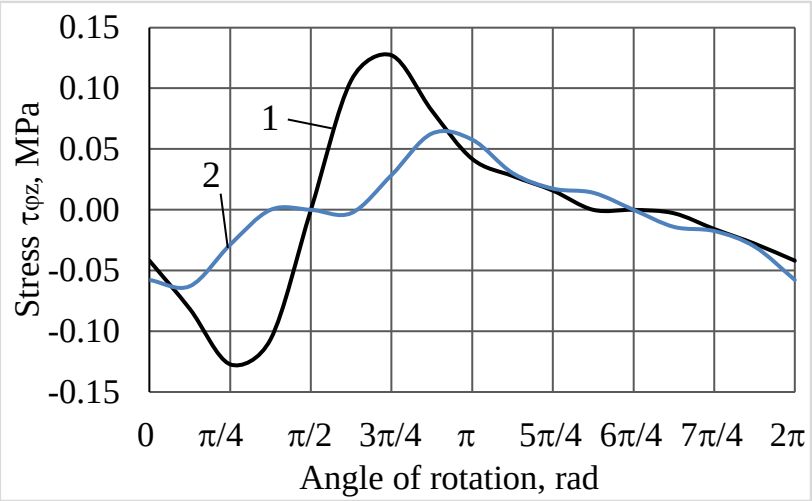

Fig. 5. Stresses $\tau_{\varphi z}$ on the pipe surfaces at a given antisymmetry: 1 – inner surface; 2 – outer surface.

It is important to note that these stresses are generated solely by the given antisymmetry of the external load, which is used to model "free end" conditions. In the case of a symmetric load (infinite layer or smooth wall), these components would be zero.

The inner surface of the pipe (Fig. 5, curve 1) shows a significantly higher amplitude of tangential stresses compared to the outer boundary. The graph has a pronounced oscillatory character with a zero crossing at π/2 (direction of the main load action). The maximum shear stress values are symmetrically located relative to this pole — near the angles 3π/8 (minimum, -0.127 MPa) and 5π/8 (maximum, +0.127 MPa). This indicates intense local "twisting" or shear of the free internal fibers of the sleeve near the edge z=0.

The tangential stresses $\tau_{\varphi z}$ on the outer surface of the pipe (Fig. 5, curve 2) are significantly lower in intensity (amplitude 0.0628 MPa) and are distributed more smoothly. Such damping of shear stresses on the outer contour is explained by the compliance of the layer matrix ($E_0 < E_1$) and the specifics of force transmission through the ideal slip surface, which partially relieves the sleeve from spatial shear.

From an engineering point of view, despite the fact that the absolute values of $\tau_{\varphi z}$ are less than the normal stresses (considered in Figs. 3 and 4), their presence near the free edge forms a complex

three-dimensional stress state. The change in sign and high gradients of these stresses can catalyze micro-sliding of the bushing and the development of fretting corrosion under cyclic operation of the hinge joint.

Fig. 6 illustrates the distribution of spatial tangential stresses $\tau_{\varphi z}$ across the thickness of the neck (bridge) between the outer surface of the reinforcing pipe (R_1 =15 mm) and the upper flat boundary of the layer (h=25 mm) under antisymmetric loading conditions. This zone, only 10 mm thick, is the site of intense superposition (interference) of edge effects from the free end, cylindrical sleeve, and flat surface of the matrix.

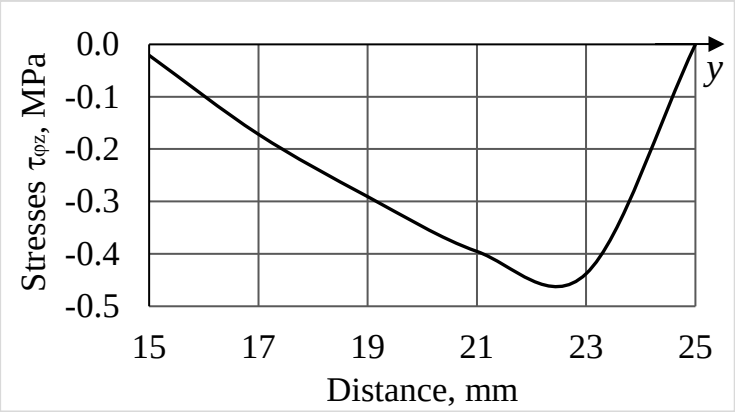

Fig. 6. Stress $\tau_{\varphi z}$ at the neck between the pipe and the upper boundary of the layer under given antisymmetry.

At the right edge of the graph (at a distance of 25 mm, corresponding to the plane $y=h$), the tangential stresses $\tau_{\varphi z}$ are exactly zero. This confirms the correctness of the analytical solution and the strict satisfaction of the boundary conditions on the free flat surfaces of the layer.

The distribution of stresses in the isthmus is extremely uneven (Fig. 6). Instead of a smooth decrease, there is a sharp increase in shear forces by modulus. The maximum concentration of tangential stresses (extremum) reaches a value of -0.43781 MPa and is localized at a distance of about 22.5 mm from the center of the system (i.e., only 2.5 mm below the upper boundary of the layer).

In the near-surface zone (between 22.5 mm and 25 mm), an extremely high gradient of stress drop from maximum to zero is recorded.

From the point of view of fracture mechanics, the detected subsurface concentration of spatial tangential stresses $\tau_{\varphi z}$in the narrow isthmus is critical. Under operating conditions (especially under cyclic or vibrational loads near the free edge), it is in this local zone that there is the highest risk of the formation of shear microcracks, their subsequent emergence on the surface, and delamination of the matrix material above the bushing. This indicates the need to increase the minimum permissible thickness of the layer above the hinge at the design stage of such assemblies.

6.3. Discussion of the results of the obtained stress state

The numerical results obtained provide a deep understanding of the physics of deformation of complex spatial structures near free or pinched boundaries. The stress state found clearly demonstrates that the presence of a vertical end face (z=0) radically changes the stress distribution pattern compared to classical models of an infinite layer. A rigid steel sleeve ($E_1 > E_0$) accumulates the load, but at the same time provokes the emergence of dangerous spatial tangential stresses $\tau_{\varphi z}$ at the boundary of smooth contact and in the thin neck of the matrix (10 mm thick).

This result is critically useful for design engineers. It explains the mechanism of failure of such joints: cracks originate not on the contact surface itself, but in the subsurface layer of the bridge, where the gradient of tangential stresses reaches its maximum due to the interference (superposition) of the edge effect and the pressure from the bushing. Using the analytical dependencies obtained, it

is possible to predict the locations of potential failure with high accuracy without the need for expensive field tests.

Existing analogues of the object under study are standard lugs, tie rod fastening nodes, and lifting mechanism boom joints, which are traditionally designed with a large margin of safety (by increasing mass) or calculated using approximate numerical packages (e.g., Ansys). The updated object (a node whose geometric parameters are optimized based on our accurate analytical model) is superior because it has reduced metal consumption due to the accurate determination of the minimum required thickness of the bridges, as well as the optimal distance from the hinge axis to the edge of the part, which prevents critical edge effects.

The application of the developed analytical and numerical methodology at the design stage significantly changes the internal factors:

– the calculation of stresses by reducing them to an infinite system of linear algebraic equations (by the reduction method) is performed in a fraction of a second, in contrast to the construction and optimization of dense 3D meshes in the finite element method;
– prototyping and trial-and-error testing costs are reduced;
– since the optimized design is lighter, its use in moving assemblies (aviation, automotive) leads to direct fuel and electricity savings during vehicle operation.

The profit from the implementation of such optimized objects is generated by extending the life cycle of the part, reducing warranty service costs, and reducing the number of sudden failures due to material fatigue.

The results of the study are extremely interesting for the world's leading technological countries (the US, Germany, Japan, China), where the giants of the aerospace and machine-building industries are concentrated. The problem of weight optimization while maintaining the strength of edge joints is a global engineering challenge.

7. Prospects for further research

The main vectors for further scientific research are:

– Complexification of coupling conditions. Transition from idealized smooth contact to modeling contact with Coulomb friction or conditions of non-ideal elastic sliding. This will allow us to assess the influence of friction forces on the redistribution of tangential stresses $\tau_{\varphi z}$ and more accurately predict areas of intense fretting wear at the "bushing-matrix" interface. It is also relevant to consider the problem with conditions of rigid coupling (hot bushing fit).

– Taking into account the heterogeneity and anisotropy of materials. Study of the stress state of structures made of modern composite or functionally graded materials (FGM), where the elastic moduli vary continuously along the coordinate. Replacing the isotropic layer with an orthotropic one will allow modeling the behavior of layered plastics or reinforced panels.

– Solving thermoelastic and dynamic problems. Integration of temperature fields into the model to estimate temperature stresses arising from friction in the joint or external heating. In addition, an important step will be the transition from statics to dynamics — the study of wave processes, diffraction of elastic waves on the sleeve and cavity under vibration or impact loads on the end face.

– Study of multicomponent systems. Extension of the method to the case of a system with an arbitrary number N of supporting pipes and cavities of different radii. This will allow optimizing multi-row bolt or rivet connections near the edge of the part, taking into account the cross-interference of stress fields from all concentrators.

– Accounting for physical nonlinearity (elastic-plastic problems). Since extreme stress concentrations have been found in the narrow isthmus between the sleeve and the layer boundary, it is promising to study the development of plastic deformation zones in this area when the yield strength of the matrix material is exceeded.

Such steps will make it possible to create a comprehensive set of engineering tools for calculating and optimizing critical components of aerospace and mechanical engineering equipment at all stages of the life cycle.

8. Conclusions

The paper solves a spatial boundary value problem of elasticity theory for determining the stress-strain state of a semi-infinite elastic layer weakened by a cylindrical cavity and reinforced by an elastic cylindrical pipe under conditions of ideal smooth contact. Based on the analytical and numerical studies, the following conclusions were made:

1. It has been proven that combining the generalized Fourier method with the mirror reflection method is a highly effective approach for studying semi-infinite bodies. The application of even or odd loads at the boundaries of an equivalent infinite layer made it possible to precisely satisfy the conditions of a "smooth wall" or "free end" on the plane z=0 without directly introducing this boundary into the solution. The application of addition theorems allowed us to reduce the boundary value problem to a regular infinite system of linear algebraic equations, which is effectively solved by the reduction method.
2. It has been established that the presence of a load-free vertical boundary (end face) radically changes the stress distribution pattern. Unlike the conditions of a "smooth wall," where stresses are distributed relatively evenly, a sharp gradient and a significant local concentration of normal stresses σ_z (more than double the increase) occur near the "free end."
3. Analysis of the stress state on the surfaces of the reinforcing pipe showed that a more rigid sleeve accumulates a significant part of the mechanical energy. At the boundary of smooth contact, radial stresses σr are transmitted continuously, but hoop stresses σ_φ undergo a sharp jump. The pipe operates under conditions of intense local bending, and in areas of maximum load, a state of triaxial compression is realized.
4. It has been proven that load antisymmetry (free end conditions) generates spatial tangential stresses $\tau_{\varphi z}$, which are absent in flat problems or under symmetrical loading. Their amplitude on the inner free surface of the pipe is significantly higher than at the contact boundary with the matrix, which can provoke micro-sliding and intensification of wear.
5. The most dangerous area in terms of strength is the narrow neck (10 mm thick) between the outer surface of the hinge and the horizontal boundary of the layer. It is here that the extreme gradient and maximum concentration of tangential stresses $\tau_{\varphi z}$ arise due to the interference of the edge effect and pressure from the bushing. This area is a potential source of subsurface shear cracks.

References:

1) Савин, Г. Н. (1968). Распределение напряжений около отверстий. Київ: Наукова думка, 891.

2) Космодамианский, А. С. (2001). Теоретическая и прикладная механика. Донецк: Донец. нац. ун-т, 210.

3) Подильчук, Ю. Н. (1979). Трехмерные задачи теории упругости. Київ: Наукова думка, 240.

4) Гринченко, В. Т., Мелешко, В. В. (1981). Гармонические колебания и волны в упругих телах. Київ: Наукова думка, 284.

5) Tekkaya, A. E., Soyarslan, C. (2014). Finite Element Method. CIRP Encyclopedia of Production Engineering. Berlin: Springer Berlin Heidelberg, 508–514. doi: http://doi.org/10.1007/978-3-642-20617-7_16699

6) Static Structural Simulation Using Ansys Discovery. Available at: https://courses.ansys.com/index.php/courses/structural-simulation

7) Fesenko, A., Vaysfel'd, N. (2019). The Wave Field of a Layer with a Cylindrical Cavity in Structural Integrity. Structural Integrity. Springer International Publishing, 277–282. doi: http://doi.org/10.1007/978-3-030-21894-2_51

8) Fesenko, A., Vaysfel'd, N. (2021). The dynamical problem for the infinite elastic layer with a cylindrical cavity. Procedia Structural Integrity, 33, 509–527. doi: http://doi.org/10.1016/j.prostr.2021.10.058

9) Khechai, A., Belarbi, M. O., Bouaziz, A., Rekbi, F. M. L. (2023). A general analytical solution of stresses around circular holes in functionally graded plates under various in-plane loading conditions. Acta Mechanica, 234, 671–691. doi: http://doi.org/10.1007/s00707-022-03413-1

10) Николаев, А. Г., Проценко, В. С. (2011). Обобщенный метод Фурье в пространственных задачах теории упругости. Харьков: Нац. аэрокосм. ун-т им. Н.Е. Жуковского «ХАИ», 344.

11) Miroshnikov, V., Denysova, T., Protsenko, V. (2019). The study of the first main problem of the theory of elasticity for a layer with a cylindrical cavity. Strength of Materials and Theory of Structures, 103, 208–218. doi: http://doi.org/10.32347/2410-2547.2019.103.208-218

12) Miroshnikov, V., Younis, B., Savin, O., Sobol, V. (2022). A linear elasticity theory to analyze the stress state of an infinite layer with a cylindrical cavity under periodic load. Computation, 10, 160. doi: http://doi.org/10.3390/computation10090160

13) Nikichanov, V. V. (2021). Determination of the stress state of a layer with a cylindrical cavity under given smooth contact conditions on the layer boundaries and displacements on the cavity surface. Proceedings of the 9th International Scientific and Practical Conference "Scientific Horizon in the Context of Social Crises". Tokyo: Otsuki Press, 208–213. Available at: https://ojs.ukrlogos.in.ua/index.php/interconf/issue/view/6-8.08.2021/569

14) Miroshnikov, V., Savin, O., Sobol, V., Nikichanov, V. (2023). Solving the problem of elasticity for a layer with N cylindrical embedded supports. Computation, 11, 172. doi: http://doi.org/10.3390/computation11090172

15) Vitaly, M. (2023). Rotation of the layer with the cylindrical pipe around the rigid cylinder. CAMPE 2021: Advances in Mechanical and Power Engineering. Cham: Springer, 314–322. doi: http://doi.org/10.1007/978-3-031-18487-1_32

16) Sverdlov, S. (2025). Determination of the stress-strain state of a bearing connection. Proceedings of the 2nd International Scientific and Practical Conference "Modern Trends in the Development of Economy, Technology and Industry". Toronto: International Scientific Unity, 229–233. Available at: https://isu-conference.com/en/archive/modern-trends-in-the-development-of-economy-technology-and-industry-12-02-25/

17) Denshchykov, O. Y. (2025). First Main Problem of the Theory of Elasticity for a Layer with Two Thick-Walled Pipes and One Cylindrical Cavity. Journal of Mechanical Engineering, 28, 44–53. doi: http://doi.org/10.15407/pmach2025.02.044

18) Kosenko, M. (2024). Solution to an elasticity problem for a layer with cylindrical embedded supports in the form of a cavity and a pipe: Rigid fixation. Proceedings of the Interdisciplinary Scientific and Practical Conference "Modern Problems of the Development of the Aerospace Industry of Ukraine: Engineering, Business, Law". Kharkiv, 170–174.

19) Ilin, O., Kosenko, M., Denshchykov, O. (2024). Analysis of the stress state of a reinforced layer with two cylindrical cavities and some contact-type conditions. Colloquium-Journal, 19, 8–13. doi: http://doi.org/10.5281/zenodo.12723815

20) Архипенко, І. О., Савін, О. Б. (2025). Концепція розв'язання задачі теорії пружності для напівнескінченого шару. 5th International Scientific and Practical Conference «Global Trends in the Development of Information Technology and Science». Stockholm, 346–348. Available at: https://isu-conference.com/wp-content/uploads/2025/01/Sweden_1_08.01.2025.pdf

21) Arkhypenko, I. O., Savin, O. B. (2025). Solution of the spatial problem of elasticity theory for a half-space shell. Colloquium-journal, 60 (253), 3–6. doi: http://doi.org/10.5281/zenodo.17013675